Wiley
European Journal of Cancer Care
Volume 2024, Article ID 8660434, 15 pages
https://doi.org/10.1155/2024/8660434

WILEY

Research Article

Construction and Validation of a Novel Prognostic T-Cell Exhaustion-Related ceRNA Network in Lung Adenocarcinoma

Hua Ye, Wenwen Yu, Xiaoqiong Bao, Yangyang Ni, Weilong Zhou, Yunlei Li, Xiangxiang Chen, Jifa Li, and Long Zheng

Department of Respiratory and Critical Care Medicine, Yueqing People's Hospital, No 338 Qingyuan Road, Chengnan Street, Yueqing 325600, Zhejiang, China

Correspondence should be addressed to Jifa Li; doctorlijifa@163.com and Long Zheng; 7270684@qq.com

Received 15 April 2024; Revised 12 July 2024; Accepted 1 August 2024

Academic Editor: Pranshu Sahgal

Background. T cell exhaustion (TEX) is a state of T cells that is characterized by poor function of effectors and increased expression of inhibitory signals. However, the heterogeneity and prognostic values of TEX in lung adenocarcinoma (LUAD) remain not fully understood. *Methods*. Based on the Cancer Genome Atlas (TCGA) and Gene Expression Omnibus (GEO) transcriptomic profiles, we screened differentially expressed lncRNAs, miRNAs, and mRNAs and identified differentially expressed TEXs. Univariate cox and LASSO regression analyses were performed to construct TEX-related prognostic signature and risk score and validated their expression using real-time PCR assay. We then investigated the potential mechanism, immune landscape, and antitumor therapy response in LUAD. *Results*. A total of 315 DE-lncRNAs, 161 DE-miRNAs, and 2589 DEGs were screened, and then 80 DE-TEXGs were identified in LUAD. Based on univariate cox and LASSO regression analyses, CCNA2 and SLC2A1 were identified as TEX-related prognostic signatures, and the risk score subsequently was calculated. LUAD patients were divided into high- and low-risk groups, and high-risk groups were involved in poor survival status, immunosuppression, and more sensitive to anti-CTLA4 therapy. Finally, a TEX-related ceRNA network was constructed and validated based on DE-lncRNAs, DE-miRNAs, and TEX-related prognostic signatures. *Conclusion*. We constructed the TEX-related prognostic signature and its relevant ceRNA network and discovered the molecular mechanism and prognostic values of TEX in LUAD.

1. Introduction

Lung cancer is the second most commonly diagnosed cancer and the leading cause of cancer-related death in the world, with 2.2 million new cases and 1.8 million deaths in 2020 [1]. Lung cancer remains the most common leading cause of cancer-related morbidity and mortality in China and has been increasing over the past decades [2, 3]. More than 80% of lung cancers are diagnosed as non-small lung cancers (NSCLCs) which mainly are consisted of lung adenocarcinoma (LUAD) and lung squamous cell carcinoma (LSCC) [4]. Despite the rapid development of medical technology, the incidence of lung cancer and the associated death rates have not decreased over time. About 70% of patients are diagnosed with lung cancer in its advanced stages, and approximately 70% to 90% of these patients have a poor five-year survival rate in China [5–8]. Therefore, early detection and treatment are essential to reduce the death rate and improving the overall survival rate of patients with lung cancer.

During acute infections or vaccinations, naive T cells were activated and differentiate into effector T cells. Following the peak of effector expansion, the resolution of inflammation, and antigen clearance, these effector T cells subsequently differentiate into memory T cells [9, 10]. However, during persistent exposure to inflammation in chronic infections and cancer, the differentiation of memory T cells is altered, leading to a state known as T cell exhaustion (TEX). The immune function of exhausted T cells can be reinvigorated [11]. TEX has been defined by poor effector function, sustained expression of multiple inhibitory receptors, and altered transcriptional states that are distinct

from the functional effector or memory T cells [12]. TEX is associated with out-of-optimal control of the tumors and inefficient response to immune checkpoint blockade (ICB) therapy [13]. A study indicates that 14 treatment-naïve NSCLC patients with states preceding exhaustion, pre-exhaustion, and exhaustion T cells are associated with a better prognosis [14]. Therefore, understanding the TEX heterogeneity in LAUD is crucial to improve the clinical outcome of treatment.

Increasing evidence indicates that noncoding RNAs, such as circular RNAs (circRNAs), PIWI-interacting RNAs (piRNAs), long noncoding RNAs (lncRNAs), and microRNAs (miRNAs), play vital roles in regulating tumorigenesis and progression of tumors [15, 16]. Commonly, lncRNAs act as decoys for miRNAs that share common miRNA response elements (MREs) to regulate the target gene expression, known as the competing endogenous RNA (ceRNA) networks [17]. ceRNAs involve in several biologic processes and contribute to carcinogenesis [18]. Long noncoding RNA LINC01287 functions as an oncogene by promoting proliferation and inhibiting apoptosis in LUAD cells through the miR-3529-5p/RNASEH2A axis under the ceNRA pattern [19]. SNHG6 also acts as ceRNA sponges miR-26a-5p regulates E2F7 expression to promote aggressive LUAD cells [20]. Additionally, the lncRNA HOXA11-AS is involved in cisplatin resistance in LUAD cells via modulating miR-454-3p/Stat3 under the ceRNA pattern [21]. However, there are still many unknowns regarding the molecular functions and regulatory mechanisms of ceRNA in LUAD.

In this study, we screened the differentially expressed transcripts, identified the TEX-related features, and construed the TEX-related prognostic signature in LUAD based on bioinformatics technologies.

2. Methods

2.1. Data Source and Processing. The transcriptome RNA sequencing (RNA-seq) data and corresponding clinical information of 507 LUAD patients and 59 normal controls, as well as microRNA sequencing (miRNA-seq) data and relevant clinical characteristics of 519 LUAD patients and 46 normal controls, were downloaded from The Cancer Genome Atlas (TCGA, https://portal.gdc.cancer.gov/). Besides, two external cohorts, GSE30219 and GSE31210 datasets, were obtained from the Gene Expression Omnibus (GEO, https://www.ncbi.nlm.nih.gov/geo/). The GSE30219 dataset includes mRNA expression profiles and relevant clinical characteristics of 293 lung cancer patients, while the GSE31210 dataset comprises mRNA expression profiles and clinical characteristics of 226 LUAD patients, both generated using the GPL570 platform. Furthermore, we retrieved the T-cell exhaustion gene (TEXG) sets from GeneCards (https://www.genecards.org/) by searching keywords "T-cell exhaustion." Ultimately, 374 TEXGs were selected based on the threshold of relevance score >3 (Table S1).

2.2. Screening of Differentially Expressed lncRNAs, miRNAs, and mRNAs. The Limma package in *R* was used to identify the differentially expressed lncRNAs (DE-lnRNAs), differentially expressed miRNAs (DE-miRNAs), and mRNAs (DEGs) between LUAD patients and normal controls, using the cutoff criteria of $|\log 2(\text{fold change, FC})| > 1$ and false discovery rate (FDR) <0.05, respectively. Subsequently, the top 50 DE-lnRNAs, top 50 DE-miRNAs, and top 50 DEGs were visualized using the pheatmap *R* package. Differentially expressed TEXGs in LUAD were obtained by intersecting DEGs with a set of 374 TEXGs.

2.3. Construction of a T-Cell Exhaustion (TEX)-Related Prognostic Signature. The Cox proportional hazards regression model (Cox model), proposed by British statistician D.R. Cox in 1972, is a semiparametric regression model. This model uses survival outcomes and survival time as dependent variables, allowing simultaneous analysis of multiple factors affecting survival duration. It can analyze data with truncated survival times and does not require specification of the survival distribution of the data. The Cox model is an important model in survival analysis [22]. Additionally, LASSO regression, also known as least absolute shrinkage and selection operator regression, is a variable selection method proposed by Robert Tibshirani in 1996. It employs penalty constraints to shrink coefficients in the fitted model. LASSO is a shrinkage estimation method where the basic idea is to minimize the sum of squared residuals under the constraint that the sum of the absolute values of the regression coefficients is less than a constant. This approach can force some regression coefficients to be exactly zero, thereby producing a parsimonious and interpretable model [23]. We constructed a TEX-related prognostic signature using the TCGA-LUAD cohort. Firstly, a univariate Cox proportional hazards regression model was performed to identify TEXGs associated with overall survival (OS), using the survival and survminer packages in *R* with a significance threshold of <0.05. Subsequently, the OS-related TEXGs were incorporated into the least absolute shrinkage and selection operator (LASSO) model to select the optimal TEXGs associated with LUAD prognosis, using the glmnet package in R. Finally, a TEX-related prognostic risk signature was constructed based on the weighted expression level and coefficient (coef) obtained from LASSO regression analysis. The risk score was calculated using the following formula, $\text{Risk score} = \sum_{i=1}^{n} \text{coef}(\text{genei}) * \text{expr}(\text{genei})$, where coef represents the regression coefficient and expr represents the expression levels of each gene derived from the LASSO regression analysis.

2.4. Evaluation of the Prognostic Values of the TEX-Related Signature. To validate the accuracy and sensitivity of the risk model, the LUAD patients in the TCGA cohort and two external cohorts (GSE30219 and GSE31210 datasets) were

stratified into high- and low-TEX-related risk groups based on the median value of risk score, determined as the optimal cutoff. The Kaplan–Meier method and log-rank test, implemented using the survival R package, were used to generate OS curves. Additionally, time-dependent receiver operating characteristic (ROC) curves for 1 year, 2 years, and 3 years were constructed using the survivalROC package in R to assess the predictive performance of the prognostic model. The area under the ROC curve (AUC) was calculated to evaluate the accuracy of the prognostic model.

2.5. Gene Set Enrichment Analysis. The KEGG pathway gene set (c2.cp.kegg.v7.4.symbols.gmt) and 50 human hallmark gene sets (h.all.v7.4.symbols.gmt) were downloaded from the Molecular Signatures Database (MSigDB, https://www.gsea-msigdb.org/gsea/msigdb/index.jsp). Gene set enrichment analysis (GSEA, https://www.broadinstitute.org/gesa/index.jsp) was then conducted to investigate the relevant biological functions between the high- and low-TEX-related risk groups. Significant pathways were identified according to the parameters of P value <0.05.

2.6. Characterization of Tumor Immune Microenvironment in LUAD between the High- and Low-Risk Groups Related to TEX. ESTIMATE package in *R* was conducted to calculate the stromal score, immune score, and ESTIMATE score of the tumor microenvironment (TME) between the high- and low-TEX-related risk group. The Estimating Relative Subsets of RNA Transcript (CIBERSORT) algorithm is a deconvolution algorithm based on an LM22 matrix file consisting of 547 genes and is used to estimate 22 immune cell types in a mixed-cell population using the gene expression files [24]. Here, we estimated the proportion of 22 immune cell types and compared their fraction between the high- and low-TEX-related risk groups using the Wilcox test. Pearson correlation analysis was conducted to assess the correlations between prognostic TEXGs and these 22 immune cell types.

2.7. Tumor Immune Dysfunction and Exclusion (TIDE) Score, Immunephenoscore (IPS) Score, and Therapy Responses. The Tumor Immune Dysfunction and Exclusion (TIDE) dysfunction score predicts the response to immune checkpoint blockade (ICB) based on two primary mechanisms of tumor immune evasion [25]. The immunephenoscore (IPS) provides a comprehensive assessment of immunogenicity [26].

Predictions of potential response to immunotherapy were also made using the Submap method available on GenePattern (https://cloud.genepattern.org/gp/pages/index.jsf). Moreover, we predicted response to drug therapy on the half-maximal inhibitory concentration (IC50) using the Genomics of Drug Sensitivity in Cancer (GDSC) database, implemented through the pRRophetic package in R. Significant differences between the high- and low-TEX-related risk groups were evaluated using the Wilcoxon test with a significance threshold of P value <0.05.

2.8. Construction of a TEX-Related ceRNA Network. For constructing the TEX-related ceRNA network, miRNA-lncRNA pairs were predicted using Starbase version 3.0 (https://starbase.sysu.edu.cn/). Additionally, the miRNA-mRNA pairs were predicted using Starbase version 3.0 (https://starbase.sysu.edu.cn/), miRcode (https://mircode.org/), miRDB (https://mirdb.org/), miRTarBase (https://mirtarbase.mbc.nctu.edu.tw/index.html), and TargetScan (https://www.targetscan.org/vert_72/). The TEX-related ceRNA network was construed based on the shared miRNAs, targets of shared miRNA, and miRNA-mRNA pairs. Finally, the ggalluvial package in R was performed to visualize the ceRNA network. OS curves were generated using the survival R package based on the optimal cutoff values of miRNA and mRNA expression from the ceRNA network to assess their prognostic significance.

2.9. Clinical Specimen. Fresh tumor tissues and adjacent nontumor tissue samples were collected from six patients at Yueqing People's Hospital Affiliated to Wenzhou Medical University between December 2023 and February 2024. All studies involving human samples were approved by the Yueqing People's Hospital Affiliated to Wenzhou Medical University ethics committee (approval number: YQYY202300216). All patients were diagnosed with LUAD and had not received any preoperative treatment. Written informed content was obtained from all participants prior to study. The tissue specimens were immediately frozen in liquid nitrogen after collection and stored at −80°C for further RNA extraction.

2.10. RNA Extraction and Real-Time PCR Assay. Total RNA was extracted with TRIzol reagent (TaKaRa, China), followed by reverse transcription was performed with PrimeScript™ RT Master Mix (TaKaRa, China) according to the manufacturer's instructions. For real-time PCR analysis, the resulting cDNA products were amplified in triplicate using TB Green® Premix Ex Taq™ (TaKaRa, China) in triplicates. U6 was employed as the internal control for normalizing miRNA expression levels, while GAPDH served as the internal control for normalizing lncRNA and gene expression levels. Relative expression was quantified by the $2^{-\Delta\Delta Ct}$ method. The primer sequences of the genes analyzed were list as follows:

GAPDH: 5′–TGTTCGTCATGGGTGTGAAC–3′ and 5′–ATGGCATGGACTGTGGTCAT–3′. U6: 5′–GCTTCGGCAGCACATATACTAAAAT–3′ and 5′–CGCTTCACGAATTTGCGTGTCAT–3′. AC012236.1: 5′–TTTGGGTTTTGGGAGCCCTT–3′ and 5′–GGGTCCTGTGCGACTGTAAA–3′. AC026401.3: 5′–CAGCGCCTTTTGCTTGTTCT–3′ and 5′–GGGCCAGATCCAAATCACCA–3′. AF131215.6: 5′–TGTTTCTGCCTCTTCACAGCA–3′ and 5′–GATATGTGGGCCGTTGTCAC-3′. AL357093.2: 5′–CCCTCTGAACCATCCCAACC-3′ and 5′–ATTTGTGCTGCTGGCATGTG–3′ LINC00261: 5′–AGGATTCTGCATGTGGGTGG–3′ and 5′–GGTGAGCCCCAGCCTTATTT–3′. LINC00665: 5′–AGAAAACACAGCAAGCCCCT–3′ and 5′–AGACTCAGGCTGATGGGGTA–3′. LINC01963: 5′–

CTTTCCAACTCCCTGGGTCC–3′ and 5′–GCCTTACC ACCCCTTGTACC–3′. LUCAT1: 5′-CTTGGCACCAGAG ACCACAA–3′ and 5′–AGCCCATGGTAGATGCTGAA C–3′. MAGI2-AS3: 5′–TGGCCATAACCAGCAGAGTG– 3′ and 5′–CAGCCCTGGTGTTTTCATGC–3′. SNHG1: 5′–ACAGCAGTTGAGGGTTTGCT–3′ and 5′–GGCTCA TGACGGGAACAGAA–3′. hsa-miR–129–5p: 5′–GGCTTT TTGCGGTCTGG–3′ and 5′–CAGTGCGTGTCGTGGAG T–3′. hsa-miR-199b–5p: 5′–GCGAGCACAGAAATTAA TACGAC–3′ and 5′–GTGCAGGGTCCGAGGT–3′. hsa-miR-218-5p: 5′–GTGCAGGGTCCGAGGT–3′ and 5′–GC GAGCACAGAATTAATACGAC–3′. CCNA2: 5′–TGAG CATGTCACCGTTCCTC–3’ and 5′–TCAGCTGGCTTC TTCTGAGC–3′. SLC2A1: 5′–GGAGCAGGTTACTACA GGGC–3′ and 5′–ATGGCTCCACCAGGGAAATG–3′.

2.11. Statistical Analysis. All statistical analyses were performed using Graphpad Prism 8.0. Data were derived from three independent experiments and are expressed as the mean ± SD (standard deviation). Student's *t*-test was employed for qRT-PCR data analysis. A significance threshold of $P < 0.05$ was used to determine statistical significance.

3. Results

3.1. Identification of the DE-lncRNAs, DE-miRNAs, and DEGs in LUAD Patients. The workflow of this study is illustrated in Figure 1. Transcriptome data of LUAD obtained from TCGA included 59 normal samples and 507 LUAD tumor samples. As shown in Figures 2(a), 2(b), and 2(c), a total of 315 DE-lncRNAs (113 upregulated and 202 downregulated, Table S2), 161 DE-miRNAs (124 upregulated and 37 downregulated, Table S3), and 2,589 DEGs (920 upregulated and 1,669 downregulated, Table S4) were identified between LUAD tumor and normal samples using the cutoff values of $|\log 2\,FC| > 1$ and $FDR < 0.05$. The top 50 DE-lncRNAs, top 50 DE-miRNAs, and top 50 DEGs are shown in Figures 2(d), 2(e), and 2(f).

3.2. Constructed a Novel TEX-Related Prognostic Signature for LUAD Patients. A total of 80 DE-TEXGs were identified by intersecting 2,589 DEGs and 374 TEXGs (Figure 3(a), Table S5). Furthermore, we conducted univariate Cox regression analysis to determine prognostic TEXGs, revealing that 23 TEXGs significantly associated with OS with a *P* value <0.05 Figure 3(b). Subsequently, two TEX-associated genes, CCNA2 and SLC2A1, were identified as the prognostic signature for LUAD patients with the lambda. min 0.068. Figures 3(c) and 3(d), Table S6.

3.3. Validation of the TEX-Related Prognostic Signature. We further validated the prognostic value of the TEX-related signature using the TCGA cohort and two external validation cohorts. As shown in Table S7, the risk score for each patient in the TCGA cohort was calculated and 507 LUAD patients were stratified into high- ($n = 164$) and low-TEX-related risk ($n = 343$) subgroups based on the median TEX-related risk score (Figure 4(a)). Similarly, patients in the external cohorts, including GSE30219 and GSE31210 cohorts, were divided into high- and low-TEX-related risk subgroups based on the median risk score Figures 4(b) and 4(c). Kaplan–Meier survival curve analysis indicated that LUAD patients in the high-TEX-related risk group had shorter overall survival times compared to those in the low-TEX-related risk group in both the training and validation cohorts Figures 4(d), 4(e), and 4(f). Additionally, time-dependent ROC curves for risk score in the TCGA cohort validated the robustness and accuracy of the prognostic risk signature, with AUC values of 0.628, 0.656, and 0.662 at 1, 2, 3 years, respectively, Figure 4(g). In the GSE30219 cohort, the AUC value for the risk score at 1, 2, 3 years were 0.621, 0.610, and 0.630, respectively, Figure 4(h). For the GSE31210 cohort, the AUC values at 1, 2, and 3 years were 0.724, 0.739, and 0.628, respectively, Figure 4(i). These findings suggest that the TEX-prognostic risk signature effectively predicts overall survival in LUAD patients.

3.4. Exploration of Biological Functions between TEX-Related Risk Groups Based on GSEA. GSEA was employed to explore the underlying differences in biological functions between high- and low-TEX-related risk groups. The results revealed enrichment of several pathways in the high- TEX-related risk group, including the cell cycle, DNA replication, nucleotide excision repair, p53 signaling, and small-cell lung cancer pathways Figure 5(a). These pathways are crucial for cellular survival, proliferation, and response to external damage. Their aberrant activity or dysregulation is closely associated with the initiation and progression of tumors. Additionally, tumor-relevant pathways such as DNA repair, E2F targets, G2M checkpoint, glycolysis, and hypoxia pathways were also enriched in the high-TEX-related risk group Figure 5(b). These pathways play crucial roles in cellular metabolism, survival, and stress response. Their abnormal activity or dysregulation is closely associated with cancer.

3.5. Characterization of Tumor Immune Microenvironment in TEX-Related Risk Groups. We also explored the immune characteristics between high- and low-TEX-related risk groups. The ESTIMATE algorithm was conducted to evaluate the stromal score, immune score, and ESTIMATE score of LUAD patients, revealing higher Immune score and ESTIMATE score in the low-TEX-related risk group compared to the high-TEX-related risk group (Figure 6(a), Table S8).

Subsequently, the CIBERSORT algorithm was performed to analyze the differences in immune cell types between the high-risk and low-risk groups. As shown in Figures 6(b) and 6(c) and Table S9, the relative proportions of resting memory CD4 T cells, resting mast cells, resting dendritic cells (DCs), T-cell regulatory (Tregs), monocyte, and memory B cell were significantly lower in high-risk than low-risk groups. Conversely, the proportions of macrophages M0, macrophages M1, activated memory

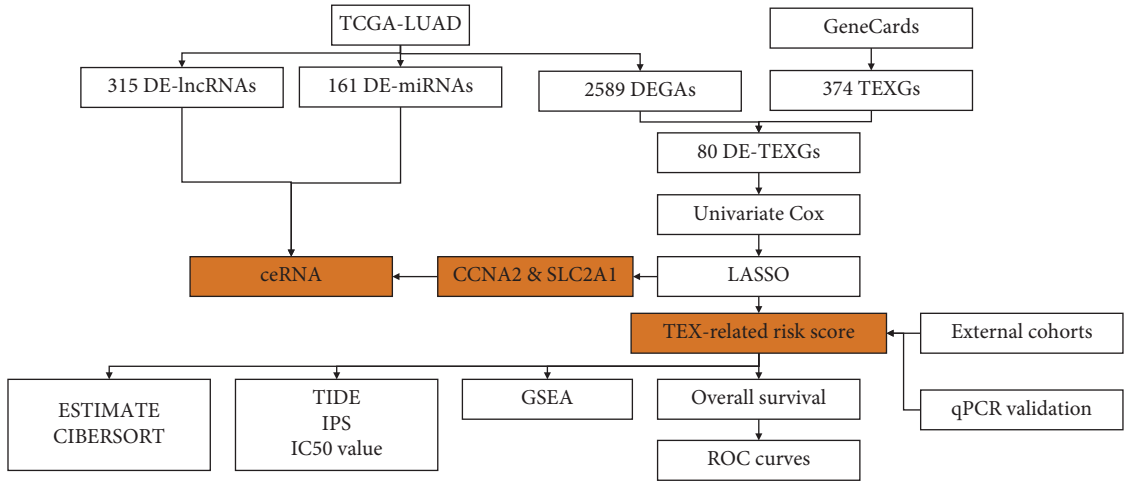

Figure 1: Flowchart of this study.

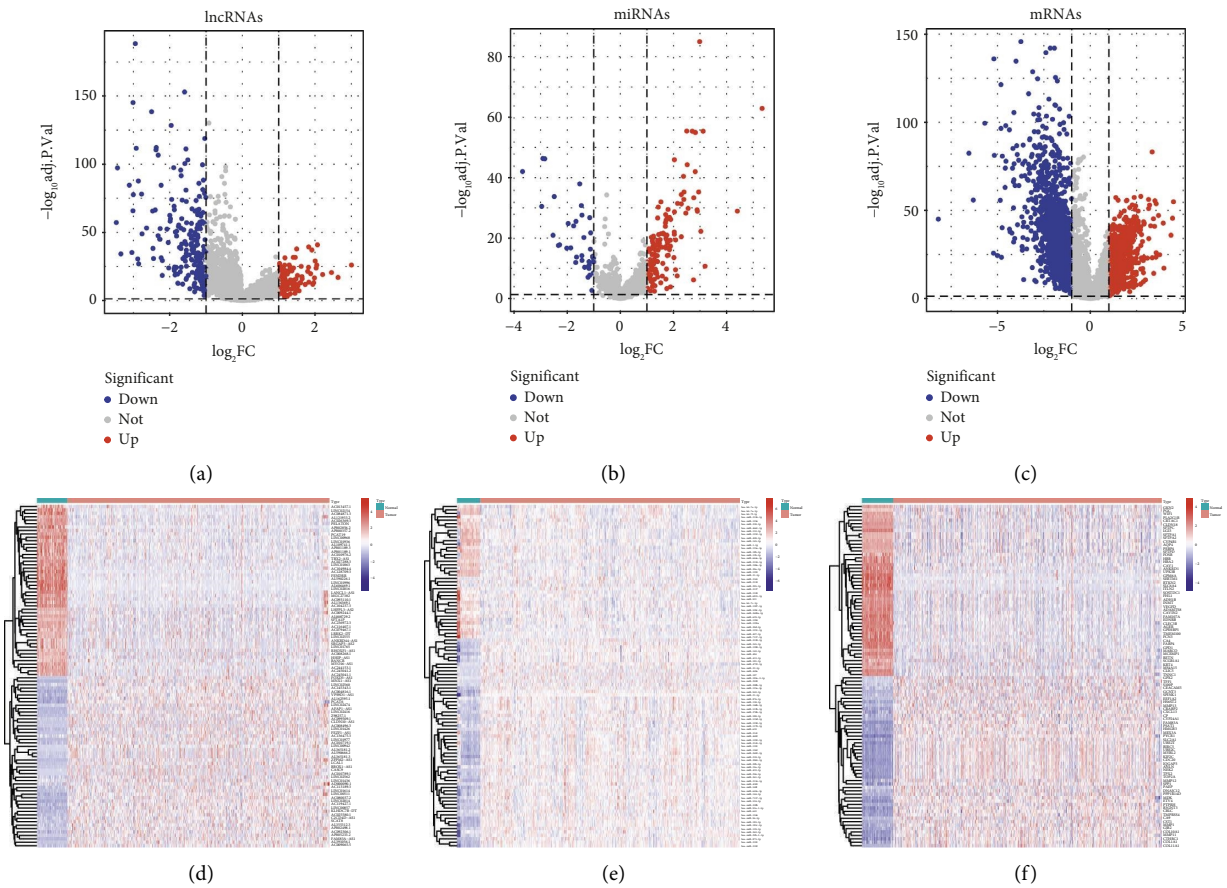

Figure 2: Identification of the DE-lncRNAs, DE-miRNAs, and DEGs in LUAD patients. (a) Volcano plot indicated the significantly differentially expressed lncRNAs (DE-lncRNAs) between LUAD tumor and normal samples. (b) Volcano plot indicated the significantly differentially expressed miRNAs (DE-miRNAs) between LUAD tumor and normal samples. (c) Volcano plot indicated the significantly differentially expressed mRNAs (DEGs) between LUAD tumor and normal samples. (d) Heatmap illustrated the top 50 DE-lncRNAs between LUAD tumor and normal samples. (e) Heatmap illustrated the top 50 DE-miRNAs between LUAD tumor and normal samples. (f) Heatmap illustrated the top 50 DEGs between LUAD tumor and normal samples.

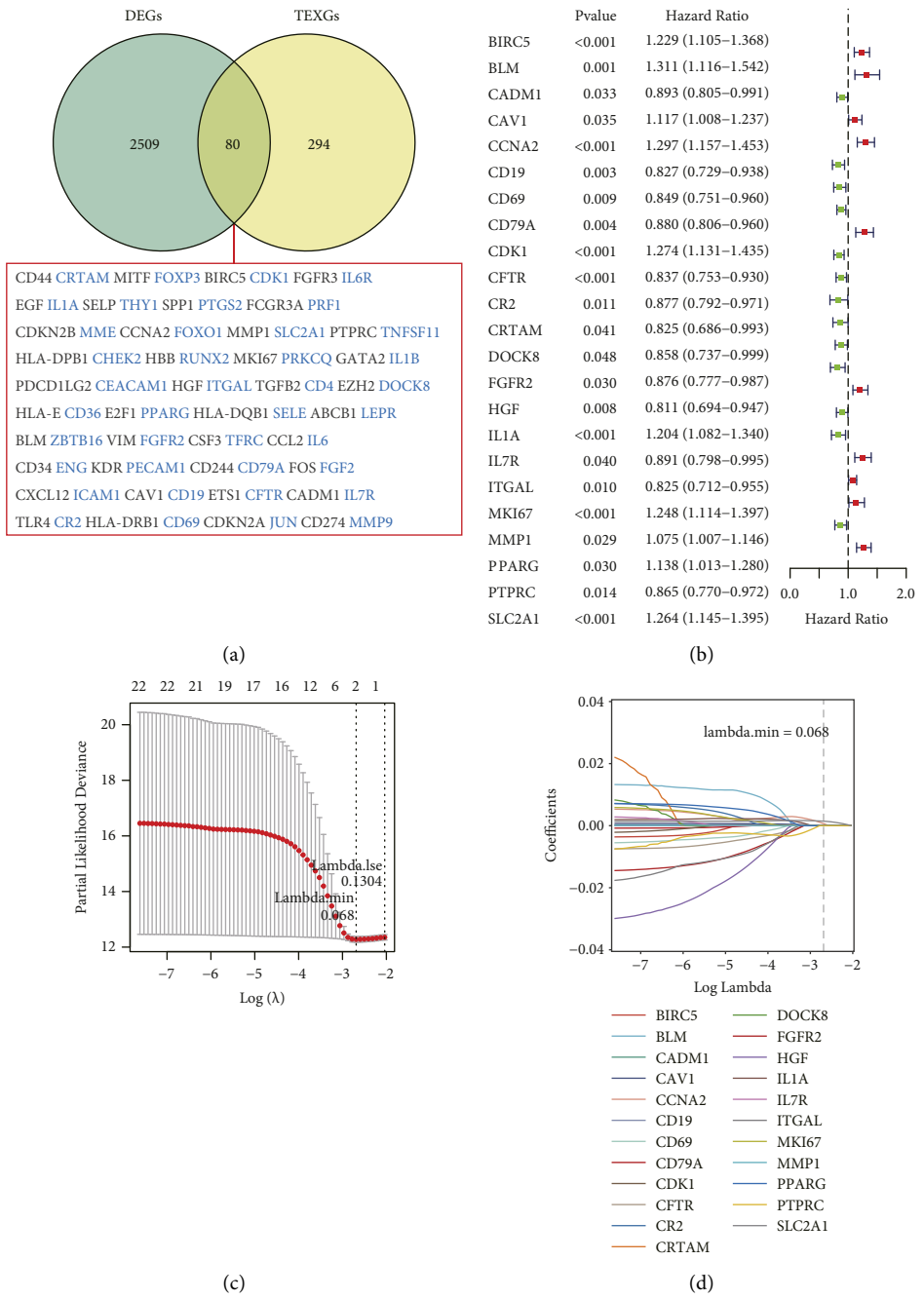

Figure 3: Constructed a novel TEX-related prognostic signature for LUAD patients. (a) Venn plot showed the differentially expressed TEXGs between LUAD tumor and normal samples. (b) Forest plot showed the OS-related TEXGs based on univariate Cox regression analysis. (c) Distribution plot of partial likelihood deviation based on LASSO regression analysis. (d) Distribution plot of the LASSO coefficient of 23 OS-related TEXGs in LUAD.

CD4T cells, neutrophils, resting NK cells, activated mast cells, and eosinophils were higher in the high-TEX-related risk group.

Furthermore, we explored the correlation between the prognostic signature and 22 types of immune cells, finding that SLC2A1 expression was positively associated with eosinophils, macrophage M0, macrophage M1, activated mast cell, neutrophils, resting NK cell, and activated memory CD4 T cells but negatively associated with memory B cell, naïve B cell, activated NK cell, and resting memory CD4 T cells (Figure 6(d), Table S10). Similarly, the expression of CCNA2 was positively associated with eosinophils, macrophage M0, macrophage M1, activated mast cell, resting NK cell, activated memory CD4 T cells, follicular delta T cells, and gamma delta T cells but negatively associated with memory B cell, activated DCs, resting DCs, resting mast cells,

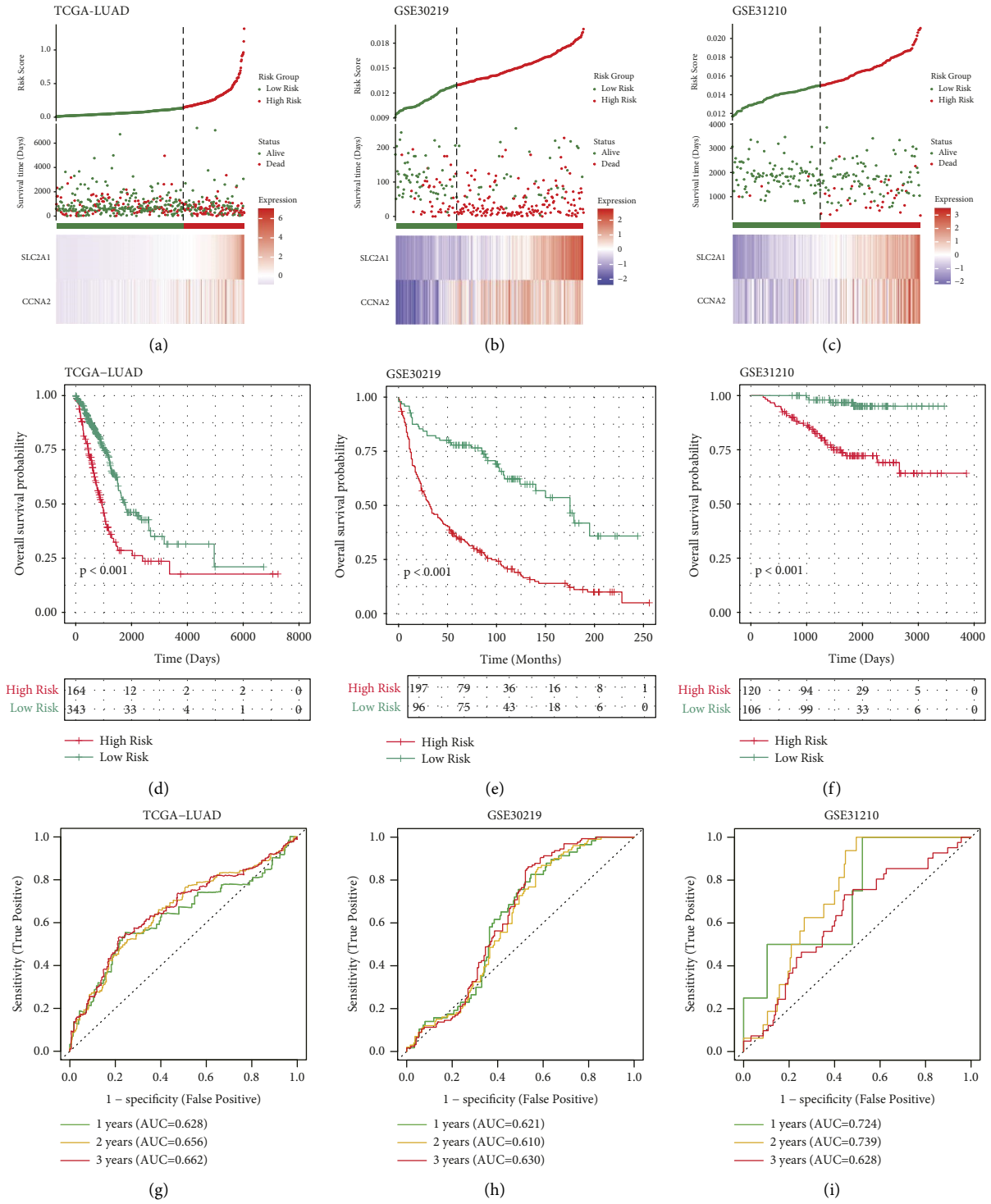

Figure 4: Validation of the TEX-related prognostic signature (a–c). Survival status distribution, risk score distribution, and the heatmap of prognostic TEXGs in TCGA-LUAD, GSE30219, and GSE31210 cohorts. (d–f). Kaplan–Meier survival curves of LUAD patients in the high- and low-TEX-related risk groups in TCGA-LUAD, GSE30219, and GSE31210 cohorts. (g–i). ROC curves for 1-, 2-, and 3-year survival of LUAD patients in TCGA-LUAD, GSE30219, and GSE31210 cohorts.

monocytes, resting memory CD4 T cells, and Tregs (Figure 6(d), Table S10). These findings indicate significant immune differences between the high-risk and low-TEX-related risk groups.

3.6. Relationship between TEX-Related Risk Score and Therapy Response in LUAD Patients. High TIDE score and low IPS score indicate the less sensitive to immunotherapy [27]. In the present study, we found a higher TIDE score in the high-

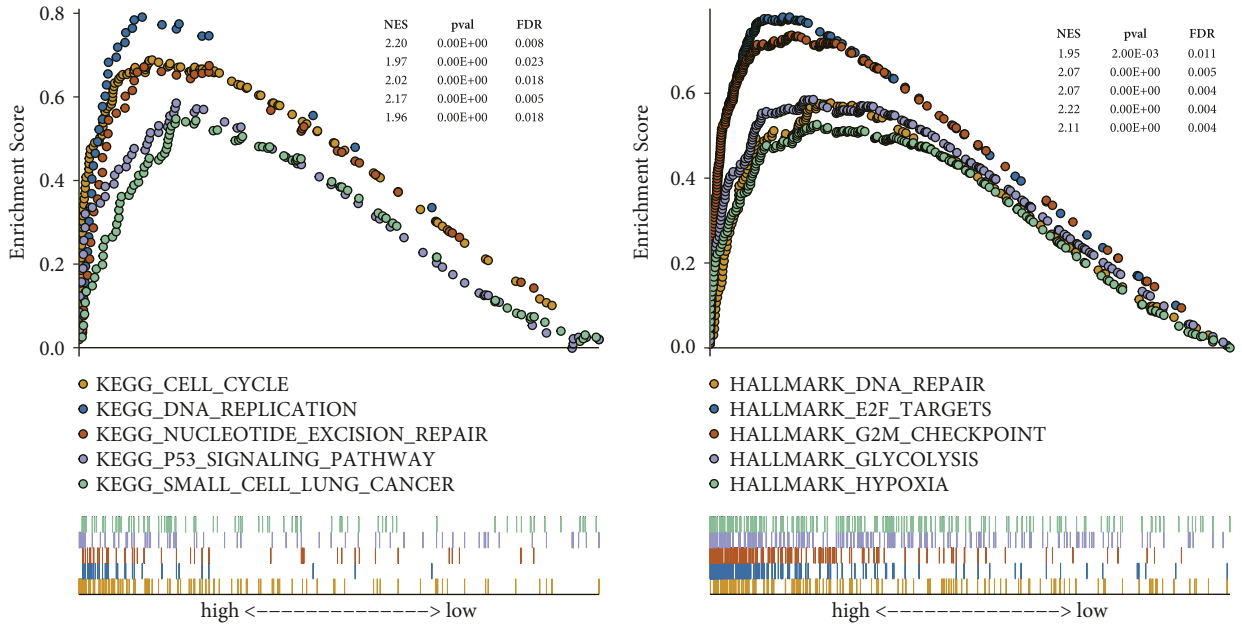

Figure 5: Exploration of biological functions between TEX-related risk groups based on GSEA. (a) GSEA indicated significantly activated KEGG pathways in the high-TEX-related risk group. (b) GSEA indicated significantly activated Hallmark pathways in the high-TEX-related risk group.

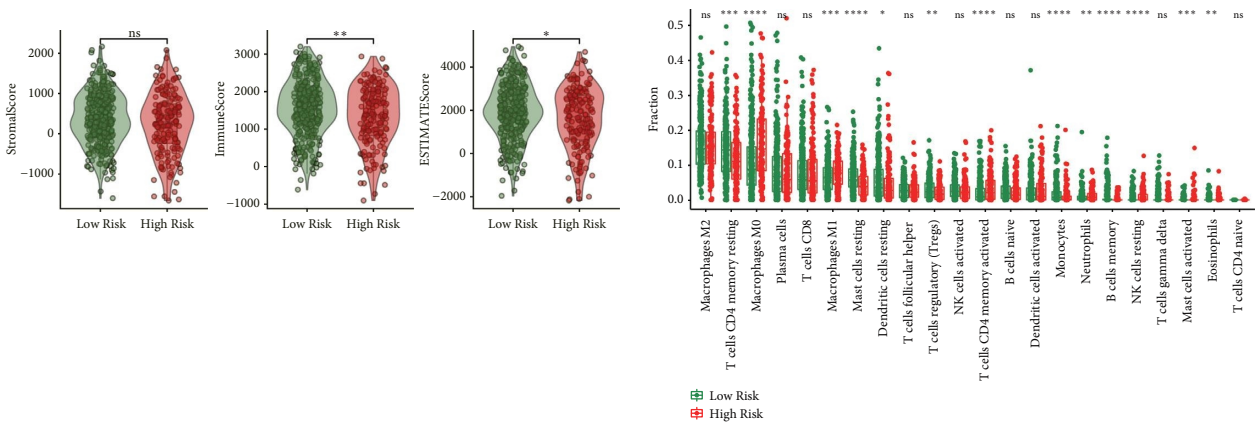

Figure 6: Continued.

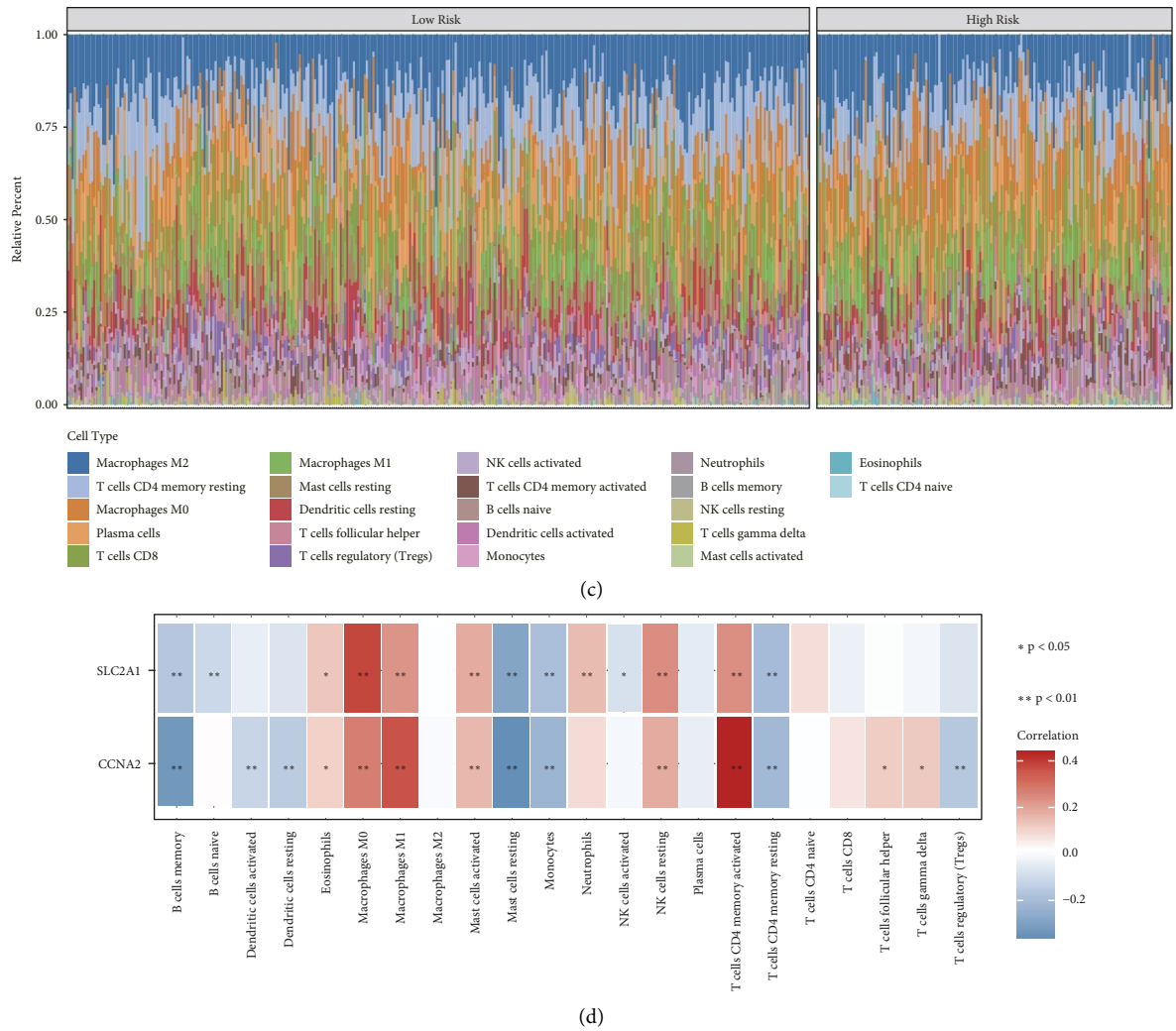

Figure 6: Characterization of the tumor immune microenvironment in TEX-related risk groups. (a) Violin plot indicated the stromal score, immune score, and ESTIMATE score between the high- and low-TEX-related risk groups. (b) Boxplots indicated differentially aggregated cells between high- and low-TEX-related risk groups. (c) Heatmap showed the distribution of 22 types of immune cells between high- and low-TEX-related risk groups. (d) Heatmap indicated the correlation between immune cells and prognostic TEXGs in LUAD.

TEX-related risk group Figure 7(a), which was positively associated with the TEX-related risk score Figure 7(b). We also found low IPS score in the high-TEX-related risk group than the low-TEX-related risk group Figure 7(c). The therapeutic response by checkpoint inhibitor blocking was then predicted based on the Submap module, resulting that the patients in the high-TEX-related risk group being more sensitive to CTLA4 inhibitors than those in the low-TEX-related risk group Figure 7(d). Additionally, sensitivity analysis of chemotherapeutics indicated higher IC_{50} values for PD-0332991, CCT007093, metformin, OSI-906, GW-441756, nutlin-3a, ABT-888, BIRB-0796, methotrexate, GDC0941, EHT-1864, lenalidomide, ATRA, MK-2206, and axitinib in the high-TEX-related risk group compared to the low-TEX-related risk group Figure 7(e). These findings suggest that the patients in a high-TEX-related risk group may exhibit increased sensitivity to anti-CTLA4 therapy but decreased sensitivity to chemotherapy compared to those in the low-TEX-related risk group.

3.7. Construction and Validation of a Novel TEX-Related ceRNA Network in LUAD. Finally, we constructed the ceRNA network to understand the regulatory mechanism of lncRNAs in LUAD. A network of TEX was constructed based on the TEX-related prognostic signature Figure 8(a), which included ten lncRNAs (AC012236.1, AC026401.3, AF131215.6, AL357093.2, LINC00261, LINC00665, LINC01963, LUCAT1, MAGI2-AS3, and SNHG1), three miRNAs (hsa-miR-129-5p, hsa-miR-199b-5p, and hsa-miR-218-5p), and two TEXGs (CCNA2 and SLC2A1). Finally, we plotted the OS curves based on the expression of three miRNAs and two TEXGs from the TEX-related ceRNA network, resulting that the LUAD patients with high levels of hsa-miR-129-5p, hsa-miR-199b-5p, and hsa-miR-218-5p showed higher overall survival time than those in low levels of hsa-miR-129-5p, hsa-miR-199b-5p, and hsa-miR-218-5p Figures 8(b), 8(c), and 8(d). The high expression of CCNA2 and SLC2A1 indicated a poorer survival time than those with low expression of CCNA2 and SLC2A1 Figures 8(e) and 8(f).

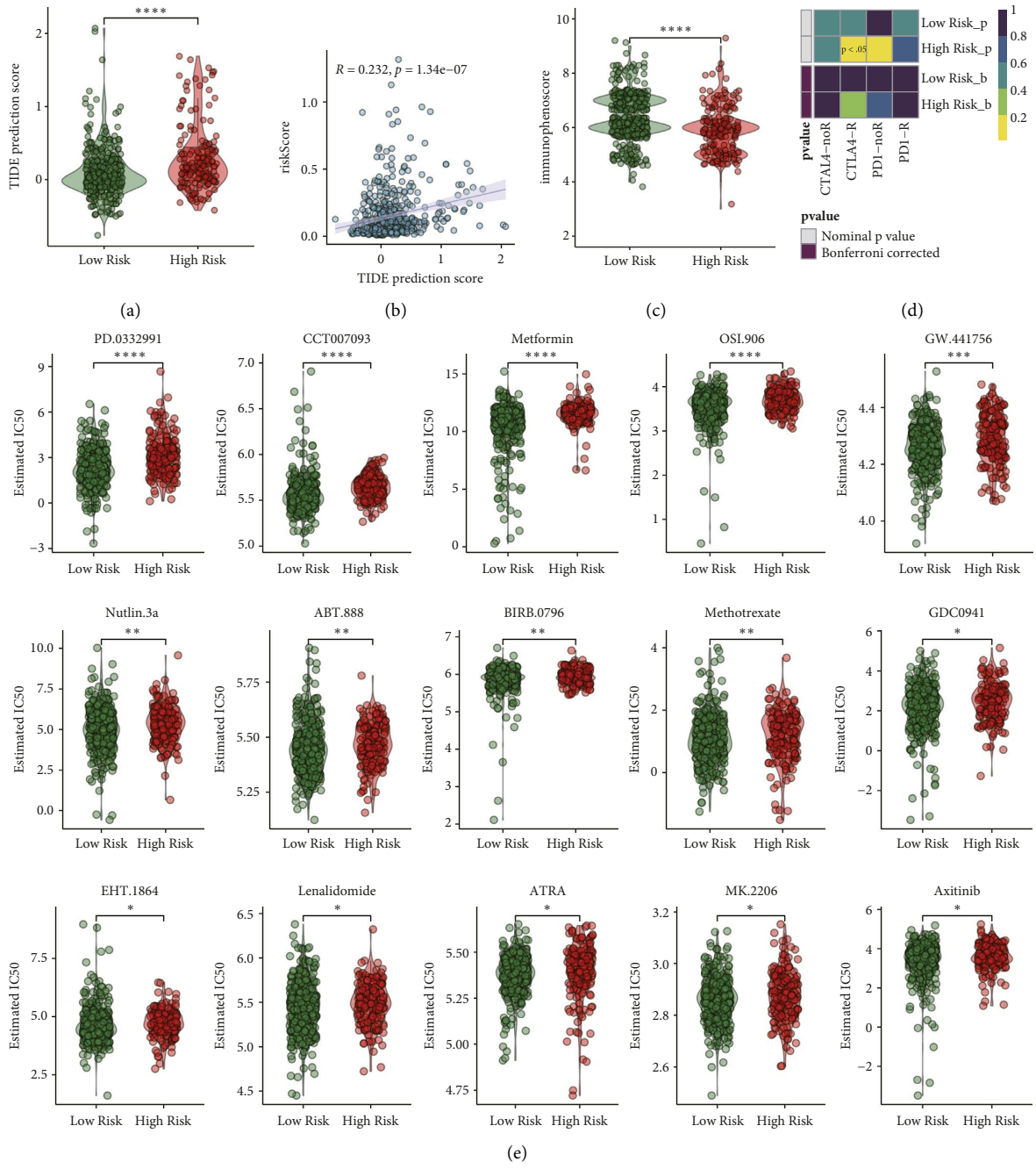

FIGURE 7: Relationship between TEXrisk score and therapy response in LUAD patients. (a) Violin plot indicated the TIDE prediction score in high- and low-TEX-related risk groups. (b) Correlation between TIDE prediction score and TEX-related risk score. (c) Violin plot indicated the IPS in high- and low-TEX-related risk groups. (d) Submap module indicated the immunotherapy response predicated for high- and low-TEX-related risk LUAD patients. (e) Violin plot indicated the chemotherapy response predicated for high- and low-TEX-related risk LUAD patients.

Furthermore, we collected the clinical specimens to validate the expression of the TEX-related ceRNA network in LUAD. As shown in Figures 9(a), 9(b), 9(c), 9(d), 9(e), 9(f), 9(g), 9(h), 9(i), and 9(j), we found the upregulated expression of AC012236.1, AC026401.3, LINC00665, LUCAT1, MAGI2-AS3, and SNHG1, while downregulated expression of AF131215.6, AL357093.2, LINC00261, and LINC01963 in LUAD tumor samples compared with adjacent normal samples. We also found the increased expression of hsa-miR-129-5p, hsa-miR-199b-5p, hsa-miR-218-5p, CCNA2, and SLC2A1 in LUAD tumor samples compared with adjacent normal samples Figures 9(k), 9(l), 9(m), 9(n), and 9(o).

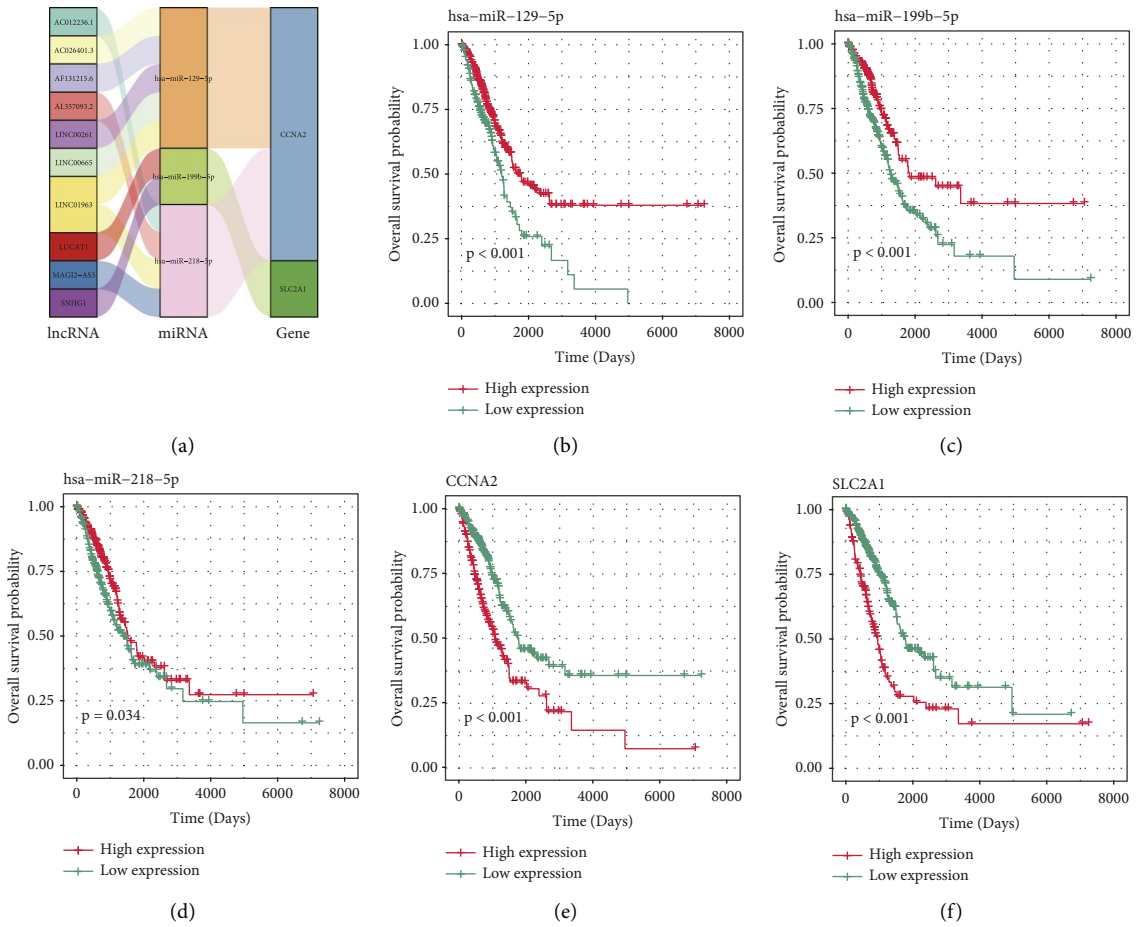

Figure 8: Construction of a novel TEX-related ceRNA network in LUAD. (a) The Sankey diagram showed the connections between ten lncRNAs (AC012236.1, AC026401.3, AF131215.6, AL357093.2, LINC00261, LINC00665, LINC01963, LUCAT1, MAGI2-AS3, and SNHG1), three miRNAs (hsa-miR-129-5p, hsa-miR-199b-5p, and hsa-miR-218-5p), and two prognostic TEXGs (CCNA2 and SLC2A1). (b–f) Kaplan–Meier survival curves of LUAD patients in the high- and low-TEX-related risk groups based on the optimal cutoff values of gene expression (hsa-miR-129-5p, hsa-miR-199b-5p, hsa-miR-218-5p, CCNA2, and SLC2A1.

4. Discussion

Cancer immune evasion poses a significant challenge in the development of effective anticancer therapies [28]. Increasing evidence suggests that TEX are associated coimmunosuppressive signals, also known as immune checkpoints, which waken T cell functions and play a crucial role in tumor immune evasion [29, 30]. Therefore, investigating TEX-related molecular characteristics in LUAD is essential to overcoming TEX and enhancing the clinical outcome of immune checkpoint blockade (ICB) therapies.

A study has identified a set of TEX risk genes using Weighted Gene Coexpression Network Analysis (WGCNA), survival random forest analysis, and LASSO regression analysis [31]. Different from this, in the present study, we identified the differentially expressed TEXGs and constructed a TEX-related prognostic signature (CCNA2 and SLC2A1) for LUAD patients using univariate and LASSO analyses. Additionally, we constructed their related ceRNA network. A TEX-related risk score was calculated, and patients were subsequently divided into high-and low-TEX-related risk groups. We found a high TEX-related risk associated with a poorer survival rate than low TEX-related risk in LUAD patients. Furthermore, several signaling pathways were enriched in the high TEX-related risk group, including cell cycle-related pathways, DNA replication and repair, nucleotide excision repair pathway, glycolysis, hypoxia pathways, and p53 signaling pathways.

CCNA2 belongs to the cell cyclin family and commonly binds to CDK2 to form a proteasome complex, thereby regulating the cell cycle [32]. CCNA2 functions as an oncogene in multiple solid tumors, and its high expression is associated with the tumor occurrence [33]. Recent research studies indicate that CCNA2 contributes to epithelial to mesenchymal transition (EMT) and is associated with metastasis in NSCLC [34, 35]. Moreover, CCNA2 is significantly correlated with poor prognosis and serves as a potential therapeutic target for LUAD [36, 37]. Our results supported the previous view that is CCNA2 acts as an oncogene and is associated with poor survival of patients in LUAD. Additionally, we highlighted the role of CCNA2 in TEX.

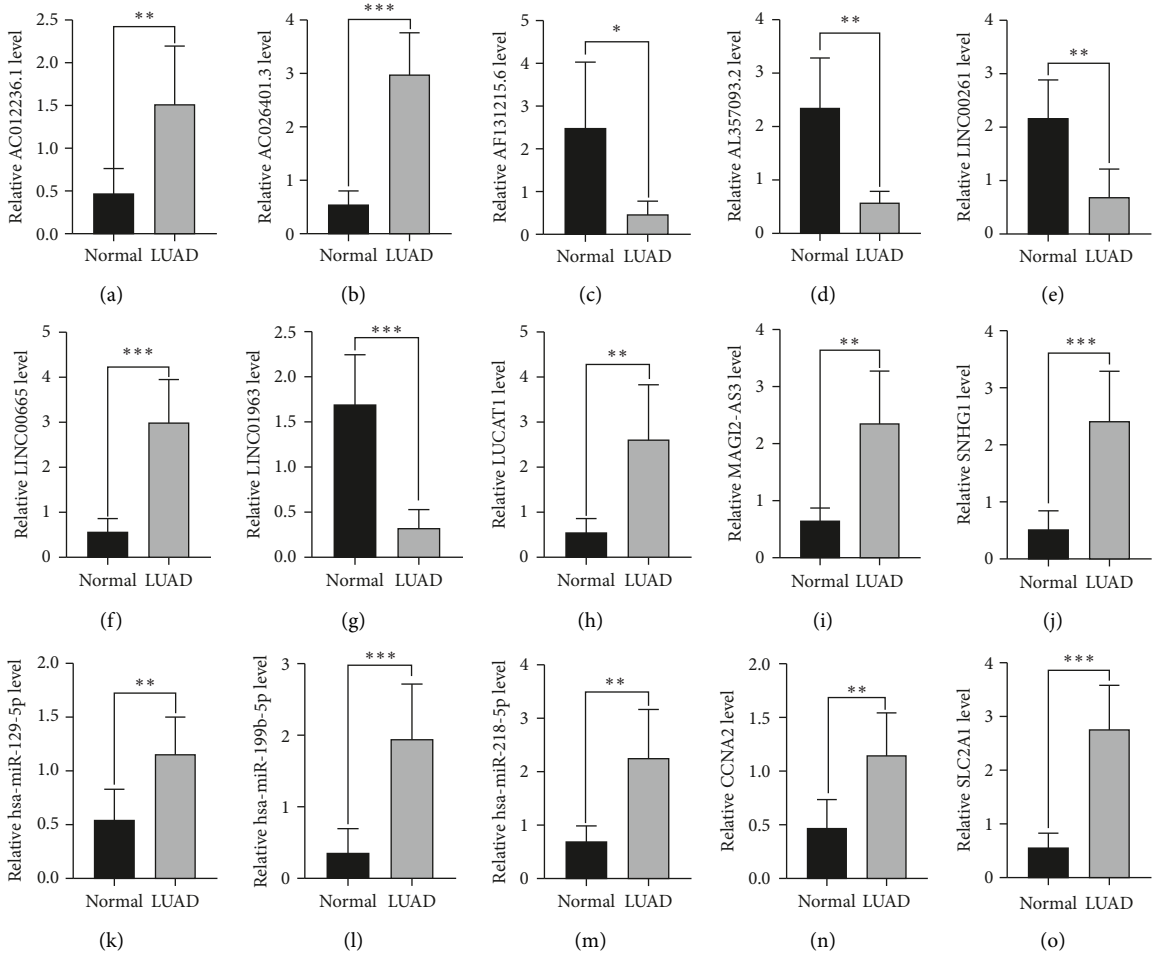

Figure 9: Real-time PCR was performed to detect the expression of TEX-related ceRNA network in LUAD. (a–o) Histograms of the relative expression of ten lncRNAs (AC012236.1, AC026401.3, AF131215.6, AL357093.2, LINC00261, LINC00665, LINC01963, LUCAT1, MAGI2-AS3, and SNHG1), three miRNAs (hsa-miR-129-5p, hsa-miR-199b-5p, and hsa-miR-218-5p), and two prognostic TEXGs (CCNA2 and SLC2A1).

Another TEX-related risk gene is SLC2A1, which encodes the glucose transporter GLUT1, playing a key role in glucose metabolism [38, 39]. Increasing studies have revealed that high expression of SLC2A1 is involved in decreased CD8 T cells and B cells in gastric cancer [40]. An *in vitro* experiment indicates that abnormal expression of GLUT1 occurs in dysfunctional memory T cells in pleural effusions secondary to lung cancer [41]. Our finding also confirmed that SLC2A1 expression is associated with TEX.

Next, we explored the immune characteristics of the tumor immune microenvironment (TIM) in LUAD. We found that high TEX-related risk was associated with low immune and ESTIMATE scores and positively correlated with inhibition of CD4 memory resting T cells, resting Mast cells, resting DCs, Tregs, monocyte, and memory B cell. Conversely, it was negatively associated with macrophages M0, macrophages M1, activated CD4 memory T cells, neutrophils, resting NK cells, activated mast cells, and eosinophils. These findings suggest that the high TEX-related risk group exhibits immune suppression, while the low TEX-related risk group shows immune activation, consistent with previous studies [42]. We investigated the correlation between TEX-related risk and immunotherapy response. Consistent with these results, we found the distinct TIDE score, IPS score, and response of anti-CTLA4 immunotherapy for LUAD. Previous studies have highlighted the crucial role of TEX in lung cancer. In the treatment of NSCLC, TEX typically exhibit high expression of inhibitory receptors such as PD-1, which limits their antitumor activity and allows tumor cells to evade immune surveillance [43]. The use of immune checkpoint inhibitors, such as anti-PD-1 and anti-PD-L1 antibodies, can partially restore the function of TEX, thereby enhancing the immune response and improving treatment outcomes for patients [44, 45]. Furthermore, the characteristics and functional states of exhausted T cells are diverse, including stem-like exhausted T cells and terminally exhausted T cells. The former possesses some proliferative capacity and self-renewal ability, while the latter exhibits higher cytotoxicity but limited proliferative capacity. These different behaviors in the tumor immune microenvironment further influence the effectiveness of immunotherapy [44, 46, 47].

Finally, we explored the regulatory mechanism of TEX-related prognostic signature (CCNA2 and SLC2A1). We identified ten lncRNAs (AC012236.1, AC026401.3, AF131215.6, AL357093.2, LINC00261, LINC00665, LINC01963, LUCAT1, MAGI2-AS3, and SNHG1) that interacted with three miRNAs (hsa-miR-129-5p, hsa-miR-199b-5p, and hsa-miR-218-5p) to regulate CCNA2 and SLC2A1 expression. This study comprehensively revealed the novel TEX-related ceRNA network for LUAD.

Although this study is the first to discover TEX-related molecular characteristics and prognostic values in LUAD and constructed the novel TEX-related ceRNA network, several limitations exist. Firstly, the functional role of the TEX-related prognostic signature should be verified using molecular experiments. Secondly, considering the complexity of multiple malignancies, the classification of TEX should be further tested and validated in other solid tumors. In the future research, we will use cell lines and animal models to explore the regulatory mechanisms of the novel TEX-related ceRNA network in LUAD.

5. Conclusion

In conclusion, we identified the differentially expressed TEXGs and then constructed the TEX-related prognostic signature to predict the prognosis of patients in LUAD. The patients were divided into two distinct TEX-related risk groups, which showed differences in survival status, immune characteristics, and response to antitumor therapy. Furthermore, we developed a novel TEX-related ceRNA network that elucidated the molecular regulatory mechanism of TEXs in LUAD.

Data Availability

The gene expression profiles and clinical data can be found at the TCGA (https://portal.gdc.cancer.gov/) and GEO (https://www.ncbi.nlm.nih.gov/geo/) databases. Software and resources used for analyses are described in each method section. And all results generated in this study are included in supplementary files.

Ethical Approval

This study was approved by the Yueqing People's Hospital Affiliated to Wenzhou Medical University Ethics Committee (approval number: YQYY202300216). All participants were known and provided informed consent.

Consent

All authors have consent for publication.

Conflicts of Interest

The authors declare that they have no conflicts of interest.

Authors' Contributions

Jifa Li and Long Zheng conceived and designed the study, Hua Ye and Wenwen Yu wrote the original draft, Xiaoqiong Bao and Yangyang Ni analyzed the data, and Weilong Zhou, Yunlei Li, and Xiangxiang Chen contributed to analysis tools. Hua Ye and Wenwen Yu contributed equally to this work.

Acknowledgments

The results here are on whole based on data generated by the TCGA and GEO databases.

Supplementary Materials

Table S1: total of 374 TEX-associated genes from GeneCards. Table S2: a total of 315 lncRNA identified between LUAD tumor and normal samples in TCGA-LUAD cohort. Table S3: a total of 161 miRNA identified between LUAD tumor and normal samples in TCGA-LUAD cohort. Table S4: a total of 2,589 DEGs identified between LUAD tumor and normal samples in TCGA-LUAD cohort. Table S5: identification of the prognostic TEXs by univariate Cox regression analysis. Table S6: identification of the prognostic signature for LUAD patients by LASSO regression analysis. Table S7: patients in the TCGA cohort were stratified into high-risk and low-risk groups based on TCGA-LUAD_riskScore. Table S8: stromal score, immune score, and ESTIMATE score of LUAD patients in TCGA-LUAD cohort by the ESTIMATE algorithm. Table S9: the 22 types of immune cells calculated by the CIBERSORT algorithm. Table S10: correlation between expression of prognostic signature and immune cells. (*Supplementary Materials*)

References

[1] H. Sung, J. Ferlay, R. L. Siegel et al., "Global cancer statistics 2020: GLOBOCAN estimates of incidence and mortality worldwide for 36 cancers in 185 countries," *CA: A Cancer Journal for Clinicians*, vol. 71, no. 3, pp. 209–249, 2021.

[2] W. Cao, H. D. Chen, Y. W. Yu, N. Li, and W. Q. Chen, "Changing profiles of cancer burden worldwide and in China: A secondary analysis of the global cancer statistics 2020," *Chinese Medical Journal*, vol. 134, no. 7, pp. 783–791, 2021.

[3] S. Gao, N. Li, S. Wang et al., "Lung cancer in people's Republic of China," *Journal of Thoracic Oncology*, vol. 15, no. 10, pp. 1567–1576, 2020.

[4] R. S. Herbst, J. V. Heymach, and S. M. Lippman, "Lung cancer," *New England Journal of Medicine*, vol. 359, no. 13, pp. 1367–1380, 2008.

[5] F. Bray, M. Laversanne, H. Sung et al., "Global cancer statistics 2022: GLOBOCAN estimates of incidence and mortality worldwide for 36 cancers in 185 countries," *CA: A Cancer Journal for Clinicians*, vol. 74, no. 3, pp. 229–263, 2024.

[6] P. Chen, Y. Liu, Y. Wen, and C. Zhou, "Non-small cell lung cancer in China," *Cancer Communications*, vol. 42, no. 10, pp. 937–970, 2022.

[7] K. Jing, H. Zhao, J. Cai et al., "The presence of autoantibodies is associated with improved overall survival in lung cancer patients," *Frontiers in Oncology*, vol. 13, 2023.

[8] Y. H. Luo, C. H. Chiu, C. H. Scott Kuo et al., "Lung cancer in Republic of China," *Journal of Thoracic Oncology*, vol. 16, no. 4, pp. 519–527, 2021.

[9] S. M. Kaech and W. Cui, "Transcriptional control of effector and memory CD8+ T cell differentiation," *Nature Reviews Immunology*, vol. 12, no. 11, pp. 749–761, 2012.

[10] D. Masopust and J. M. Schenkel, "The integration of T cell migration, differentiation and function," *Nature Reviews Immunology*, vol. 13, no. 5, pp. 309–320, 2013.

[11] E. J. Wherry, "T cell exhaustion," *Nature Immunology*, vol. 12, no. 6, pp. 492–499, 2011.

[12] E. J. Wherry and M. Kurachi, "Molecular and cellular insights into T cell exhaustion," *Nature Reviews Immunology*, vol. 15, no. 8, pp. 486–499, 2015.

[13] J. S. Dolina, N. Van Braeckel-Budimir, G. D. Thomas, and S. Salek-Ardakani, "CD8(+) T cell exhaustion in cancer," *Frontiers in Immunology*, vol. 12, 2021.

[14] X. Guo, Y. Zhang, L. Zheng et al., "Global characterization of T cells in non-small-cell lung cancer by single-cell sequencing," *Nature Medicine*, vol. 24, no. 7, pp. 978–985, 2018.

[15] H. Yan and P. Bu, "Non-coding RNA in cancer," *Essays in Biochemistry*, vol. 65, no. 4, pp. 625–639, 2021.

[16] X. Zhang, K. Xie, H. Zhou et al., "Role of non-coding RNAs and RNA modifiers in cancer therapy resistance," *Molecular Cancer*, vol. 19, no. 1, p. 47, 2020.

[17] J. J. Chan and Y. Tay, "Noncoding RNA:RNA regulatory networks in cancer," *International Journal of Molecular Sciences*, vol. 19, no. 5, p. 1310, 2018.

[18] F. A. Karreth and P. P. Pandolfi, "ceRNA cross-talk in cancer: When ce-bling rivalries go awry," *Cancer Discovery*, vol. 3, no. 10, pp. 1113–1121, 2013.

[19] J. Zhang, D. Ma, H. Kang, J. Zhao, and M. Yang, "Long noncoding RNA LINC01287 promotes proliferation and inhibits apoptosis of lung adenocarcinoma cells via the miR-3529-5p/RNASEH2A axis under the competitive endogenous RNA pattern," *Environmental Toxicology*, vol. 36, no. 10, pp. 2093–2104, 2021.

[20] R. Liang, G. Xiao, M. Wang et al., "SNHG6 functions as a competing endogenous RNA to regulate E2F7 expression by sponging miR-26a-5p in lung adenocarcinoma," *Biomedicine and Pharmacotherapy*, vol. 107, pp. 1434–1446, 2018.

[21] X. Zhao, X. Li, L. Zhou et al., "LncRNA HOXA11-AS drives cisplatin resistance of human LUAD cells via modulating miR-454-3p/Stat3," *Cancer Science*, vol. 109, no. 10, pp. 3068–3079, 2018.

[22] D. Cox, "Regression models and life-tables," *Journal of the Royal Statistical Society*, vol. 34, no. 2, pp. 187–202, 1972.

[23] R. Tibshirani, "Regression shrinkage and selection via the lasso," *Journal of the Royal Statistical Society*, vol. 58, no. 1, pp. 267–288, 1996.

[24] A. M. Newman, C. L. Liu, M. R. Green et al., "Robust enumeration of cell subsets from tissue expression profiles," *Nature Methods*, vol. 12, no. 5, pp. 453–457, 2015.

[25] P. Jiang, S. Gu, D. Pan et al., "Signatures of T cell dysfunction and exclusion predict cancer immunotherapy response," *Nature Medicine*, vol. 24, no. 10, pp. 1550–1558, 2018.

[26] K. B. Givechian, K. Wnuk, C. Garner et al., "Identification of an immune gene expression signature associated with favorable clinical features in Treg-enriched patient tumor samples," *Npj Genomic Medicine*, vol. 3, no. 1, p. 14, 2018.

[27] Y. Gao, X. Zhang, Y. Li et al., "A novel pyroptosis-related signature predicts prognosis and indicates immunotherapy in oral squamous cell carcinoma," *Journal of Cancer Research and Clinical Oncology*, vol. 149, no. 13, pp. 12057–12070, 2023.

[28] D. S. Vinay, E. P. Ryan, G. Pawelec et al., "Immune evasion in cancer: mechanistic basis and therapeutic strategies," *Seminars in Cancer Biology*, vol. 35, pp. S185–s198, 2015.

[29] J. M. Pitt, M. Vétizou, R. Daillère et al., "Resistance mechanisms to immune-checkpoint blockade in cancer: Tumor-intrinsic and -extrinsic factors," *Immunity*, vol. 44, no. 6, pp. 1255–1269, 2016.

[30] D. Saka, M. Gökalp, B. Piyade et al., "Mechanisms of T-cell exhaustion in pancreatic cancer," *Cancers*, vol. 12, no. 8, p. 2274, 2020.

[31] P. Hu, J. Ma, and J. Chen, "A systematic and comprehensive analysis of T cell exhaustion related to therapy in lung adenocarcinoma tumor microenvironment," *Frontiers in Pharmacology*, vol. 14, 2023.

[32] J. Wu, Q. Lv, J. He et al., "MicroRNA-188 suppresses G1/S transition by targeting multiple cyclin/CDK complexes," *Cell Communication and Signaling*, vol. 12, no. 1, p. 66, 2014.

[33] J. Casado-Vela, J. L. Martínez-Torrecuadrada, and J. I. Casal, "Differential phosphorylation patterns between the Cyclin-A2/CDK2 complex and their monomers," *Protein Expression and Purification*, vol. 66, no. 1, pp. 15–21, 2009.

[34] L. J. Du, L. J. Mao, and R. J. Jing, "Long noncoding RNA DNAH17-AS1 promotes tumorigenesis and metastasis of non-small cell lung cancer via regulating miR-877-5p/CCNA2 pathway," *Biochemical and Biophysical Research Communications*, vol. 533, no. 3, pp. 565–572, 2020.

[35] J. S. Ruan, H. Zhou, L. Yang, L. Wang, Z. S. Jiang, and S. M. Wang, "CCNA2 facilitates epithelial-to-mesenchymal transition via the integrin $\alpha v\beta 3$ signaling in NSCLC," *International Journal of Clinical and Experimental Pathology*, vol. 10, no. 8, pp. 8324–8333, 2017.

[36] Y. Huang, L. Zhong, K. Nie et al., "Identification of LINC00665-miR-let-7b-CCNA2 competing endogenous RNA network associated with prognosis of lung adenocarcinoma," *Scientific Reports*, vol. 11, no. 1, p. 4434, 2021.

[37] Z. Li, Y. Zhang, Y. Zhou et al., "Tanshinone IIA suppresses the progression of lung adenocarcinoma through regulating CCNA2-CDK2 complex and AURKA/PLK1 pathway," *Scientific Reports*, vol. 11, no. 1, 2021.

[38] B. Thorens and M. Mueckler, "Glucose transporters in the 21st century," *American Journal of Physiology. Endocrinology and Metabolism*, vol. 298, no. 2, pp. E141–E145, 2010.

[39] A. Yamada, K. Oguchi, M. Fukushima, Y. Imai, and M. Kadoya, "Evaluation of 2-deoxy-2-[18F]fluoro-D-glucose positron emission tomography in gastric carcinoma: relation to histological subtypes, depth of tumor invasion, and glucose transporter-1 expression," *Annals of Nuclear Medicine*, vol. 20, no. 9, pp. 597–604, 2006.

[40] K. W. Min, D. H. Kim, B. K. Son et al., "High SLC2A1 expression associated with suppressing CD8 T cells and B cells promoted cancer survival in gastric cancer," *PLoS One*, vol. 16, no. 3, p. e0245075, 2021.

[41] H. Prado-Garcia, S. Romero-Garcia, D. A. Castro-Flores, and U. Rumbo-Nava, "Deficient glucose uptake is linked to impaired Glut1 expression upon CD3/CD28 stimulation in memory T cells from pleural effusions secondary to lung cancer," *Scandinavian Journal of Immunology*, vol. 90, no. 3, p. e12802, 2019.

[42] K. Shimizu, T. Iyoda, M. Okada, S. Yamasaki, and S. I. Fujii, "Immune suppression and reversal of the suppressive tumor

microenvironment," *International Immunology*, vol. 30, no. 10, pp. 445–455, 2018.

[43] A. Chow, K. Perica, C. A. Klebanoff, and J. D. Wolchok, "Clinical implications of T cell exhaustion for cancer immunotherapy," *Nature Reviews Clinical Oncology*, vol. 19, no. 12, pp. 775–790, 2022.

[44] A. E. Brunell, R. Lahesmaa, A. Autio, and A. K. Thotakura, "Exhausted T cells hijacking the cancer-immunity cycle: assets and liabilities," *Frontiers in Immunology*, vol. 14, 2023.

[45] A. Chow, K. Perica, C. A. Klebanoff, and J. D. Wolchok, "Clinical implications of T cell exhaustion for cancer immunotherapy," *Nature Reviews Clinical Oncology*, vol. 19, no. 12, pp. 775–790, 2022.

[46] M. Hashimoto, K. Araki, M. A. Cardenas et al., "PD-1 combination therapy with IL-2 modifies CD8(+) T cell exhaustion program," *Nature*, vol. 610, no. 7930, pp. 173–181, 2022.

[47] C. Y. Hu, Y. H. Zhang, T. Wang et al., "Interleukin-2 reverses CD8+ T cell exhaustion in clinical malignant pleural effusion of lung cancer," *Clinical and Experimental Immunology*, vol. 186, no. 1, pp. 106–114, 2016.